Infrared Spectrum of the Propargyl Peroxyl Radical, HC≡C−CH_2OO $\tilde{X}$ $^2A''$†

Evan B. Jochnowitz,[‡,§] Xu Zhang,[‡,∥] Mark R. Nimlos,[‡,⊥] Bradley A. Flowers,[‡,#] John F. Stanton,[▽] and G. Barney Ellison*[,‡]

Department of Chemistry & Biochemistry, University of Colorado, Boulder, Colorado 80309-0215, Institute for Physical Chemistry, University of Basel, Klingelbergstrasse 80, CH-4056 Basel, Switzerland, Jet Propulsion Laboratory, California Institute of Technology, 4800 Oak Grove Drive, Pasadena, California 91109-8099, National Renewable Energy Laboratory, 1617 Cole Boulevard, Golden, Colorado 80401, Earth and Environmental Sciences Division, Los Alamos National Laboratory, Mail Stop D462, Los Alamos, New Mexico 87545, and John F. Stanton, Institute for Theoretical Chemistry, Department of Chemistry, University of Texas, Austin, Texas 78712

Received: August 12, 2009; Revised Manuscript Received: September 18, 2009

When the propargyl radical, $HCCCH_2$, and O_2 are codeposited onto a cold argon matrix, a chemical reaction ensues; infrared absorption spectra reveal the formation of the propargyl peroxyl radical: $HC\equiv\dot{C}-\dot{C}H_2$ $\tilde{X}$ $^2B_1$ + O_2 → *trans*-HC≡C−CH_2OO $\tilde{X}$ ^2A We do not observe the isomeric adduct, CH_2=C=CHOO $\tilde{X}$ $^2A''$. The propargyl radicals are produced by a hyperthermal nozzle while a second nozzle alternately fires bursts of O_2/Ar at the 20 K matrix. The absorption spectra of the radicals are measured using a Fourier transform infrared spectrometer. We observe 13 of the 18 fundamental infrared bands of the propargyl peroxyl radical in an Ar matrix at 20 K. The experimental frequencies (cm^{-1}) of *trans*-HC≡C−CH_2OO $\tilde{X}$ $^2A''$ are assigned. The a′ modes are $\nu_1 = 3326$, $\nu_2 = 2960$, $\nu_3 = 2148$, $\nu_4 = 1440$, $\nu_5 = 1338$, $\nu_6 = 1127$, $\nu_7 = 982$, $\nu_8 = 928$, $\nu_9 = 684$, and $\nu_{10} = 499$ cm^{-1}, while the a″ modes are $\nu_{14} = 1218$, $\nu_{15} = 972$, and $\nu_{16} = 637$ cm^{-1}. Linear dichroism spectra were measured with photo-oriented $HCCCH_2OO$ radical samples to establish the experimental polarizations of several vibrational bands. The experimental frequencies (ν) for the propargyl peroxyl radical are compared to the anharmonic frequencies (υ) resulting from electronic structure calculations. We have used CBS-QB3 electronic structure calculations to estimate the peroxyl bond energies: ΔH_{298}(*trans*-HC≡CCH_2−OO → CH_2CCH $\tilde{X}$ $^2B_1$ + O_2) = 19 ± 1 kcal mol^{-1} and ΔH_{298}(*trans*-CH_2=C=CH−OO → CH_2CCH $\tilde{X}$ $^2B_1$ + O_2) = 21 ± 1 kcal mol^{-1}. The experimental thermochemistry for C_3H_3 reacting with oxygen has been reanalyzed as $\Delta_{rxn}H_{298}$($HCCCH_2$ + O_2 → CH_2=C=O + HCO) = −83 ± 3 kcal mol^{-1}; $\Delta_{rxn}H_{298}$($HCCCH_2$ + O_2 → CH_3CO + CO) = −111 ± 3 kcal mol^{-1}; $\Delta_{rxn}H_{298}$($HCCCH_2$ + O_2 → CH_2CHO + CO) = −106 ± 4 kcal mol^{-1}; $\Delta_{rxn}H_{298}$($HCCCH_2$ + O_2 → HCHO + HCCO) = −67 ± 4 kcal mol^{-1}; $\Delta_{rxn}H_{298}$($HCCCH_2$ + O_2 → CH_2CH + CO_2) = −105 ± 3 kcal mol^{-1}.

Introduction

The propargyl radical ($HCCCH_2$) is an important species in combustion.[1,2] This species is produced[2] in flames by H abstraction from either $CH_3C\equiv CH$ or CH_2=C=CH_2 or by the addition of CH_2 $\tilde{a}$ $^1A_1$ to HC≡CH. Propargyl is a delocalized hydrocarbon radical and is classically written[3] as [HC≡C−CH_2 ↔ HC=C=CH_2]. The spin-delocalization on $HCCCH_2$ has been measured and it has been shown that there is a significant amount of spin density on either side of the propargyl molecule. An EPR spectrum of propargyl revealed a "doublet of triplets" in its hyperfine splitting pattern, indicating comparable spin densities [(spin)(atom)$^{-1}$] on the (1,3) carbons.[4] CCSD(T)/ANO spin density calculations[5] based on coupled-cluster theory find 35% of the spin on C(3) and 65% on C(1). The $HCCCH_2$ radical is a doublet and can be represented by$HC\equiv\dot{C}-\dot{C}H_2$ $\tilde{X}$ $^2B_1$ corresponding to the generalized valence bond (GVB) diagrams[6] in eq 1.

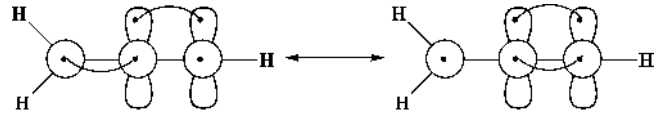

35 % $\tilde{X}$ $^2B_1$ CH_2CCH (propargyl radical) 65 % (1)

From hydrocarbon thermochemistry[7] one can show that the delocalized propargyl radical is stabilized[5] by approximately 11 kcal mol^{-1} (the "resonance energy"). And it has already been emphasized[2] that $HCCCH_2$ forms weak bonds with oxygen since O_2 addition destroys the resonance. Weakly bound [C_3H_3OO]* adducts do not readily rearrange to produce oxidized bimolecular products and are not stabilized by collisions. Many of the [C_3H_3OO]* dissociate back to O_2 + C_3H_3. Consequently propargyl radicals begin to reach high concentrations in flames and react with themselves[2,8] to form aromatic species: $HCCCH_2$ + $HCCCH_2$ → C_6H_6 → (benzene).[8–12]

† Part of the "W. Carl Lineberger Festschrift".

* To whom correspondence should be addressed. E-mail: barney@jila.colorado.edu.
‡ University of Colorado.
§ University of Basel.
∥ California Institute of Technology.
⊥ National Renewable Energy Laboratory.
Los Alamos National Laboratory.
▽ University of Texas.

10.1021/jp907806g
Published on Web 12/29/2009

Although dimerization may be the dominant loss channel for propargyl radicals in flames, reactions with oxygen will certainly play a crucial role as well.[2,10,13,14] Possible reaction channels for propargyl and oxygen are

$$HC\dddot{=}C\dddot{-}CH_2 + O_2 \rightarrow CH_2{=}C{=}O + HCO \quad (2)$$

$$\rightarrow CH_3CO + CO \quad (3)$$

$$\rightarrow CH_2CHO + CO \quad (4)$$

$$\rightarrow CH_2O + HCCO \quad (5)$$

$$\rightarrow CH_2CH + CO_2 \quad (6)$$

In a pioneering study, the kinetics and mechanism of the reaction of C_3H_3 with O_2 were investigated[13] from 293 to 900 K using a tubular reactor coupled to a photoionization mass spectrometer (PIMS). The flow reactor was a 1.05 cm-id heatable quartz tube with N_2 buffer gas at pressures of 0.9−1.8 Torr. From 293−333 K, the reaction is a simple, reversible addition: $C_3H_3 + O_2 \rightleftharpoons C_3H_3OO$. Between 380 and 430 K the equilibrium was clearly observable and the equilibrium constant was measured as a function of temperature. The binding energy of oxygen to propargyl, $\Delta H_{298}(C_3H_3{-}OO)$, was deduced[13] to be 18.9 ± 1.4 kcal mol^{-1}. A mechanism change was observed as the temperature rises. Above 350 K, $CH_2{=}C{=}O + HCO$ are observed as reaction products and remain important as the temperature increases.

Laser photolysis (193 nm) and cavity ring-down spectroscopy were used[10] to produce and monitor the propargyl radical. The oxygen termolecular association rate coefficients for the propargyl radical were measured at 295 K at total pressures between 2.25 and 100 Torr in Ar, He, and N_2 buffer gases. The association reaction $C_3H_3 + O_2$ was found to lie in the falloff region between linear and saturated pressure dependence for each buffer gas (Ar, He, and N_2). A fit of these data derived the high-pressure limiting rate coefficient $k_\infty(C_3H_3 + O_2) = (2.3 \pm 0.5) \times 10^{-13}$ cm^3 molecule^{-1} s^{-1}.

In addition to the earlier[13] flow tube/PIMS study, the reaction dynamics of propargyl radical with O_2 was studied at low pressures by time-resolved Fourier transform infrared (FTIR) spectroscopy.[14] A gas mixture of $HCCCH_2Br$ (0.3 Torr) and O_2 (0.2 Torr) was flowed through a reaction chamber. The $HCCCH_2$ radical was produced by laser photolysis of C_3H_3Br at 248 nm and the reaction of propargyl radical with O_2 was observed. Emission of infrared radiation was observed from the nascent vibrationally excited products HCO*, CO_2*, and CO* after 5 μs following laser triggering by time-resolved FTIR spectroscopy. Observation of these products led to the conclusion that reactions 2, 3, and 6 are the dominant channels for $HCCCH_2$ reacting with O_2.

Hahn et al.[2] carried out a theoretical study of the temperature and pressure-dependent kinetics of the reaction of propargyl radical with molecular oxygen. They calculated the stationary points on the potential energy surfaces for the addition of O_2 with $HC\dddot{=}C\dddot{-}CH_2$ $\tilde{X}\,^2B_1$ by a combination of electronic structure theory, transition state theory, and the time-dependent master equation. The stationary points on the potential energy surface were located with B3LYP density functional methods. QCISD(T,full)/6-311++G(3df,2pd) energies were obtained at these stationary points.

An important question is the nature of the initial addition complex because there are two isomeric adducts possible.

$$HC\dddot{=}C\dddot{-}CH_2 + O_2 \rightarrow CH_2{=}C{=}CH{-}OO\cdot \quad (7)$$

$$HC\dddot{=}C\dddot{-}CH_2 + O_2 \rightarrow HC{\equiv}C{-}CH_2{-}OO\cdot \quad (8)$$

QCISD(T) electronic structure calculations[2] find there is a lower barrier for the addition of O_2 to the methylenic side of the radical to form $HC{\equiv}CCH_2{-}OO\cdot$ [$E_a(8) = 3.7$ kcal mol^{-1}] than to the acetylenic end to produce the more stable[2] $CH_2{=}C{=}CH{-}OO\cdot$ [$E_a(7) = 7.1$ kcal mol^{-1})] adduct. Those barriers suggest that molecular oxygen would preferentially react with propargyl radicals to form $HC{\equiv}CCH_2OO\cdot$ rather than $CH_2{=}C{=}CH{-}OO\cdot$. The order of these barriers, $E_a(8) < E_a(7)$, reflects the spin densities on the propargyl radical in eq 2.

More than a decade ago it was demonstrated that a hyperthermal nozzle could decompose propargyl bromide to produce intense beams of the radical.[15]

$$HC{\equiv}C{-}CH_2{-}Br + \Delta \rightarrow HC\dddot{=}C\dddot{-}CH_2 + Br \quad (9)$$

Using such a hyperthermal nozzle we have produced an intense beam of propargyl radicals and measured their vibrational spectra when deposited upon a cold (20 K) argon matrix using an FTIR spectrometer.[5] Polarizing 248 nm light from a KrF excimer laser enabled us to record linear dichroism spectra of photooriented samples, thus establishing the experimental polarizations of most of the vibrational bands. Of the 12 fundamental vibrational modes of propargyl, 9 were observed.

Our earlier study[16] shows that it is possible to combine CH_3 radicals with O_2 in at Ar matrix to produce the methylperoxyl radical, CH_3OO. Because of this earlier success, we have codeposited samples of $HCCCH_2$ and O_2 in a cryogenic matrix. Infrared absorption spectroscopy has been used to identify reaction products. The IR spectra reveal that the reaction product of $HCCCH_2$ $\tilde{X}\,^2B_1$ with O_2 in a 20 K Ar matrix is the propargyl peroxyl radical, *trans*-$HC{\equiv}C{-}CH_2OO\cdot$ $\tilde{X}\,^2A''$. We find no evidence for the isomeric allenyl peroxyl radical, $CH_2{=}C{=}CH{-}OO\cdot$ $\tilde{X}\,^2A''$.

Experimental Section

Radical Beam and Infrared Spectroscopy. We use a hyperthermal nozzle to produce intense beams of propargyl radical.[5] Briefly, the nozzle consists of a resistively heated 1-mm diameter SiC tube at the output of a pulsed solenoid Parker General Valve (Series 9). The hyperthermal nozzle can be heated up to 1800 K to thermally dissociate an appropriate precursor. Because the radical's residence time in the hyperthermal nozzle is approximately 65 μs, few radical−radical byproducts are observed. Upon exiting the nozzle the hot molecules undergo a supersonic expansion since they are entrained by the Ar buffer gas. Two different propargyl radical precursors were used in this work: $HC{\equiv}CCH_2Br$ and $HC{\equiv}CCH_2CH_2ONO$. The propargyl bromide precursor was purchased from Aldrich Chemical Co., while 1-butyn-4-nitrite ($HC{\equiv}CCH_2CH_2ONO$) was synthesized.[5] The nitrite is a convenient source of propargyl radical because the hyperthermal nozzle fragments the nitrite at a lower temperature than $HC{\equiv}CCH_2Br$. An estimate[17] for the bond energy is $\Delta H_{298}(HCCCH_2CH_2O{-}NO)$ roughly 42 kcal mol^{-1}.

$$HC{\equiv}C{-}CH_2{-}CH_2{-}O{-}N{=}O + \Delta \rightarrow$$
$$[HCCCH_2CH_2O + NO] \rightarrow HC{\equiv}\dot{C}{-}\dot{C}H_2 + CH_2O + NO \quad (10)$$

The hyperthermal nozzle was optimized for propargyl radicals by use of a combination of photoionization mass spectrometry and infrared spectroscopy.[5]

The hyperthermal nozzle was mounted to the vacuum shroud of an APD two-stage closed-cycle helium cryostat, approximately 2.5 cm away from the cryogenic CsI sample.[18] Room temperature gas mixtures were created by seeding the degassed vapor of the precursor in argon. The hyperthermal nozzle was operated with an approximate 150 μs pulse width and a stagnation pressure of 1.2 atm. The pressure drop in the stagnation reservoir (1.2 L) was measured using a capacitance monometer to determine the gas throughput.

Propargyl peroxyl radicals were produced by mixing O_2 and propargyl radicals in the matrix, in a similar fashion to the technique used by Nandi et al.[16] to create the methylperoxyl radical, CH_3OO. The method consists of first depositing propargyl radicals from the pyrolysis nozzle. A second Parker General Valve Series 9 pulsed solenoid valve then introduces the O_2/Ar gas mixture to the matrix. This second valve mounts to the same APD vacuum shroud, positioned 45° from the pyrolysis nozzle and also approximately 2.5 cm away from the cryogenic CsI substrate. One beam was dosed at a time onto the 20 K window; by depositing alternating monolayers of reactants a multilayer sandwich matrix is created. Both valves were fitted with 100 μm circular output orifices.

The infrared spectrum of the sample was measured after dosing the matrix substrate for approximately one hour using a Nicolet Magna 550 Fourier transform infrared spectrometer with a mercury/cadmium/telluride (MCT-A or B) detector. The APD cryostat is equipped with a pair of CsI side windows that are traversed by the IR beam. For depletion and linear dichroism experiments a KrF excimer laser and a plate polarizer were used to produce polarized 248 nm light to create an aligned matrix of trapped propargyl peroxyl radicals. Subsequently the difference in the IR signal was obtained with the light first polarized horizontally and then vertically. This yields the linear dichroism spectrum of the matrix. Polarized IR light is generated with a Molectron wire grid IR polarizer.

Electronic Structure Calculations. The vibrational assignments were facilitated using harmonic frequencies calculated from electronic structure methods. The equilibrium geometry and harmonic frequencies of $HCCCH_2OO$ and CH_2CCHOO species were calculated using a commercial computer program that employs the B3LYP functional which is a combination of exchange from Becke's 3-parameter HF/DFT hybrid exchange functional[19] (B3) with the dynamical correlation functional[20] of Lee, Yang, and Parr (LYP).

To estimate the bond energies of $HCCCH_2{-}OO$ and $CH_2CCH{-}OO$, we have used the complete basis set (CBS) methods developed by Petersson et al.[21,22] These compound models employ modest basis sets for the geometry and frequency calculations, large basis sets for a single point SCF calculation, medium basis sets for the MP2 correction with extrapolation to the CBS limit, and small basis sets for higher levels of correlation. The CBS-QB3 method[22] uses the CBS-Q model chemistry that has been modified to use B3LYP hybrid density functional geometries and harmonic frequencies $\{\omega\}$ and has a characteristic accuracy of ± 1 kcal mol^{-1}.

Coupled-cluster theory,[23–26] while more expensive than DFT methods, provides a nearly quantitative treatment of electron correlation in most cases and can therefore provide accuracy beyond that achievable with DFT. Accordingly, we have used another package[27] (CFOUR) to calculate the equilibrium geometry, anharmonic force field, and dipole moment function for propargyl peroxy using the CCSD(T) method[28,29] with the atomic natural orbital (ANO) basis set.[30] The anharmonic force field $\{v\}$ was calculated by numerical differentiation of analytical CCSD(T) second derivatives[31] using a general approach described elsewhere.[32] Care was taken to ensure that the numerical precision of the frequencies (harmonic and anharmonic) quoted in Table 1 is roughly 1 cm^{-1}. The core molecular orbitals corresponding to the 1s carbon atomic orbitals were excluded from the correlation treatment. For propargyl peroxy,

TABLE 1: Calculated *trans*-H−C≡C−CH_2−OO $\tilde{X}\,^2A''$ Vibrational Modes CCSD(T) Calculation of Harmonic (ω) and Anharmonic (v) Vibrational Frequencies and Intensities for *trans*−H−C≡C−CH_2−OO $\tilde{X}\,^2A''$ Using the ANO0 Basis Set[a]

mode	local mode	ω (cm^{-1})	v (cm^{-1})	$v-\omega$ (cm^{-1})	A(ω) (km mol^{-1})	A(v) (km mol^{-1})	v (adj)	A (adj)
a′								
1	C−H st	3466	3332	−134	50	45	3337	44
2	sym CH_2 st	3092	2961	−131	7	7	2951	7
3	C≡C st	2169	2126	−43	6	4	2144	5
4	CH_2 scissors	1490	1453	−37	3	1	1445	2
5	CH_2 wag	1374	1339	−35	50	41	1336	42
6	O−OCH_2CCH st	1086	1072	−14	26	10	1130[b]	20[b]
7	C−C st	986	967	−19	18	16	973	20
8	O−C st	976	933	−43	27	50	943	65
9	C≡C−H in-plane bend	667	652	−15	31	31	678	32
10	O−C−C bend	499	487	−12	3	2	496	2
11	O−O−C bend	418	416	−2	9	9	424	9
12	C−C≡C in-plane deformation	157	155	−34	1	1	163	1[c]
a″								
13	asym CH_2 st	3155	2994	−161	4	4	2980	5
14	CH_2 twist	1231	1197	−34	1	1	1189	1
15	CH_2 rock	1002	977	−25	4	4	973[d]	4[d]
16	C≡C−H out-plane bend	623	608	−15	40	40	633	42
17	C−C≡C out-plane deformation	293	296	3	6	7	309	7
18	O−O−CH_2−C torsion	79	72	−7	0	0	73	0

[a] "Adjusted" values in the rightmost columns are based on the CCSD(T)/ANO1 harmonic force field (see the section Electronic Structure Calculations) and represent the best estimates from theory. [b] After treatment of $\nu_6 \simeq \nu_9 + \nu_{11}$ resonance. [c] After treatment of $\nu_{12} \simeq 2\nu_{18}$ resonance. [d] After treatment of $\nu_{15} \simeq \nu_9 + \nu_{17}$ resonance.

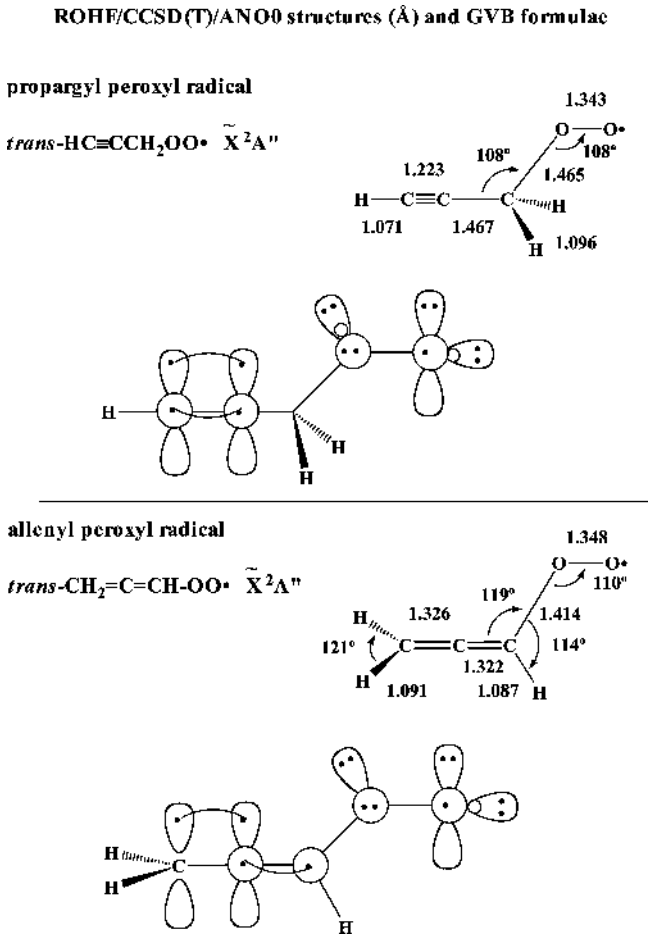

Figure 1. Minimized C_3H_3OO geometries found resulting from an ROHF/CCSD(T)/ANO0 calculation. The two minimum structures are the *trans*-propargyl peroxyl radical, HC≡C−CH_2OO $\tilde{X}\,^2A''$, and the *trans*-allenyl peroxyl radical, CH_2=C=C−OO $\tilde{X}\,^2A''$. All distances are in Å and angles are in degrees. GVB structures[6] are shown as well.

the harmonic force field was obtained with both the 4s2p1d (on H)/4s3p2d1f (on C) contraction known as ANO1 and the somewhat smaller 2s1p (H)/3s2p1d (C) contraction called ANO0. The anharmonic force field was determined only with the smaller basis, and the fundamental levels were calculated with second-order vibrational perturbation theory (VPT2) using the ANO1 harmonic force field in conjunction with cubic and quartic constants obtained with CCSD(T)/ANO0.

Results

One anticipates several isomers of the C_3H_3OO radical: *cis*- and *trans*-HC≡CCH_2OO as well as *cis*- and *trans*-CH_2=C=CHOO. Both peroxyl radicals have $\tilde{X}\,^2A''$ ground states; Figure 1 shows the GVB structures.[6] To determine the structure and energy of the C_3H_3OO product, electronic structure calculations were performed using the B3LYP/6-311G(d,p) and CCSD(T)/ANO methods. Four isomers of C_3H_3OO were calculated: *cis*- and *trans*-HC≡CCH_2OO, as well as *cis*- and *trans*-CH_2=C=CHOO. The *trans*-CH_2=C=CHOO isomer was identified as the most stable conformation, while *cis*-HC≡CCH_2−OO never converged as a stable minimum but to a gauche structure located more than 2 kcal mol^{-1} below the cis conformer. For all structures the CCC angle was nearly 180°. Minima for both cis and trans conformations were found for the CH_2=C=CHOO peroxyl, as well as *trans*- and *gauche*-HC≡C−CH_2OO. Anharmonic frequencies for HC≡C−CH_2OO were calculated from the optimized geometry in Figure 1 and are summarized in Table 1.

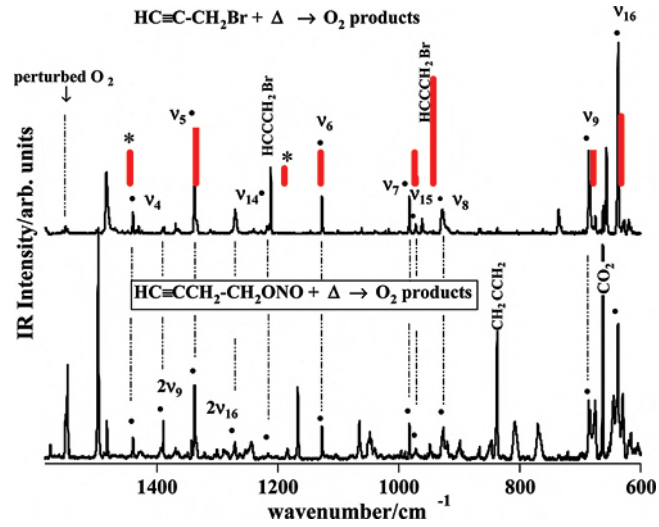

Figure 2. IR spectra of the propargyl peroxyl resulting from addition of $HCCCH_2$ radicals to O_2 in an Ar matrix at 20 K. Propargyl radicals are produced from two different precursors. The top spectrum is propargyl peroxyl radical generated by using HC≡C−CH_2Br as a precursor for propargyl radicals, while the bottom spectrum is a spectrum of propargyl peroxyl radical using HC≡C−CH_2CH_2ONO as a precursor. The calculated CCSD(T)/ANO anharmonic frequencies $\{v\}$ are shown as sticks in red while the experimental frequencies $\{\nu\}$ are marked by bullets (•). Peaks common to both spectra are attributed as being due to the C_3H_3OO adduct, unless otherwise noted.

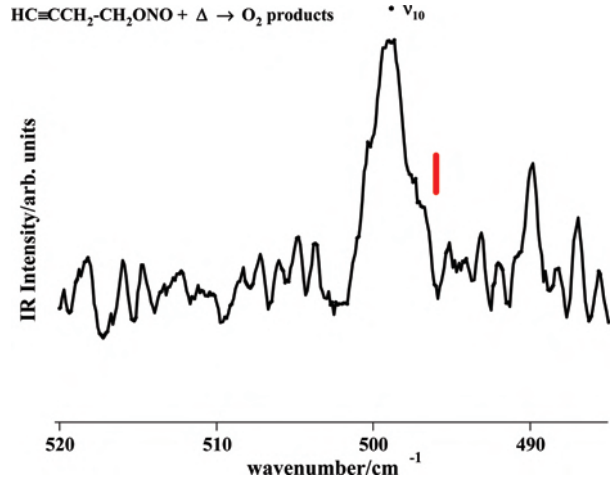

Figure 3. The OO−CH_2−CCH bending mode (ν_{10}) of HC≡CCH_2OO radical that results for addition of $HCCCH_2$ radical to oxygen. Propargyl radicals are generated by thermal cracking of HC≡C−CH_2CH_2ONO.

Figure 2 shows the fingerprint region of the C_3H_3OO radical, 1600−600 cm^{-1}. The bottom trace represents C_3H_3OO formed by condensing O_2 with $HCCCH_2$ produced by decomposition of HC≡C−CH_2CH_2ONO (bottom trace) and HC≡C−CH_2Br (top trace). Common bands exhibiting similar relative intensity patterns are assigned to the HC≡CCH_2OO radical. These assignments are guided by the anharmonic frequencies predicted by the CCSD(T) calculation in Table 1. The computed *trans*-HC≡CCH_2−OO stick spectrum, shown in red, closely resembles the experimental spectrum. The only C_3H_3OO peak observed below 600 cm^{-1} was generated from HC≡C−CH_2CH_2ONO and is shown in Figure 3. Figure 4 depicts the CH stretching region while Figure 5 shows the −C≡C− region. Figures 6, 7, and 8 display the remaining low frequency bands. In all of these

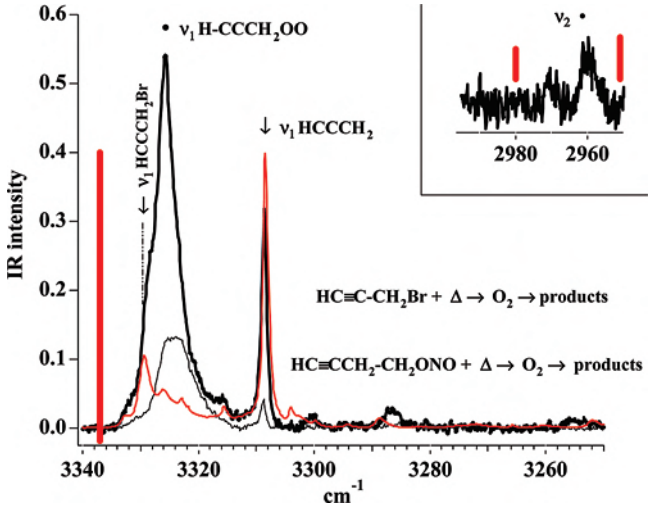

Figure 4. The two black traces are IR spectra (of the CH stretching region) resulting from combination of propargyl radicals with O_2 in a cryogenic matrix. The top black trace uses $HCCCH_2Br$ as the propargyl precursor and the bottom trace uses $HCCCH_2CH_2ONO$ to generate propargyl radical. The red trace is the IR spectrum that results from the thermal cracking of $HC{\equiv}C{-}CH_2Br$. The red spectrum provides us with $\nu_1(H{-}CCCH_2Br)$ and $\nu_1(H{-}CCCH_2)$. The intense red stick is the predicted CCSD(T)/ANO anharmonic transition, υ_1. The in-set at the top of the figure shows the weak CH_2 absorption at 2960 cm^{-1} resulting from reaction of propargyl radical (from $HCCCH_2Br$) and oxygen. The red stick is the predicted CCSD(T)/ANO υ_2 at 2951 cm^{-1}.

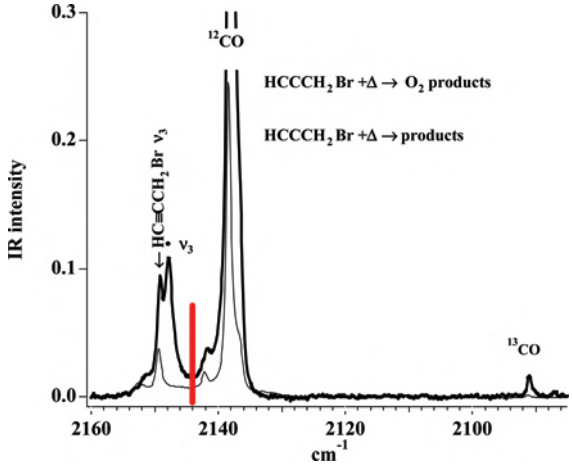

Figure 5. A scan through the $-C{\equiv}C-$ stretching region of the IR spectrum following the addition of $HCCCH_2$ to O_2. The top black trace uses $HCCCH_2Br$ as the propargyl precursor together with addition of O_2. The bottom trace is of $HCCCH_2Br$ and the $HCCCH_2$ radical by themselves; no oxygen is present. The intense red stick is the predicted CCSD(T)/ANO anharmonic transition, $\upsilon_3(HC{\equiv}CCH_2OO)$.

figures, the predicted CCSD(T) anharmonic modes $\{\upsilon\}$ from Table 1 are plotted as red sticks.

Linear dichroism spectra were also measured to aid in the assignment of vibrational bands. The electronic structure of all alkyl peroxyl radicals should be somewhat similar, because their electronic transitions tend to be localized on the terminal oxygen atoms. For both HOO and CH_3OO the ground state[33,34] is $\tilde{X}\,^2A''$. The low lying $\tilde{A}\,^2A'$ excited states of a handful of peroxyl radicals have been extensively studied, with the $\tilde{A}\,^2A'-\tilde{X}\,^2A''$ transitions lying in the near IR.[35–39] Alkyl peroxyl radicals also possess a second, dissociative, excited state with broad electronic transitions usually in vicinity of 260 nm ($\tilde{B}\,^2A''-\tilde{X}\,^2A''$). Consequently the transition matrix element $\langle \tilde{B}\,^2A''\,|\mu|\,\tilde{X}\,^2A''\rangle$ yields the symmetry of the transition moment to be A′. As a first step the initially isotropic distribution of propargyl peroxyl radicals trapped in the matrix is selectively depleted using polarized 248 nm light until roughly 75% of the identified $HCCCH_2{-}OO$ IR fundamental lines are bleached. Because the laser is polarized horizontal with respect to the laboratory frame, Z, any propargyl peroxyl molecule with a significant projection of its transition dipole moment, μ, parallel to the depleting laser light is destroyed because of excitation to the broad $\tilde{B}\,^2A''$ dissociative state (200−300 nm). The remaining propargyl peroxyl radicals are therefore oriented with their transition dipole moments perpendicular to the depleting laser light and the molecules in the matrix are aligned. Depletion spectra are shown as the black traces in Figures 9 and 10.

Linear dichroism spectra are then collected with polarized IR light generated using a Molectron wire grid IR polarizer. The difference in the two polarized spectra collected with the light parallel and perpendicular with respect to the laboratory frame (I_Z-I_Y) yields the LD spectrum of the aligned matrix species, shown as the red traces in Figures 9−11.

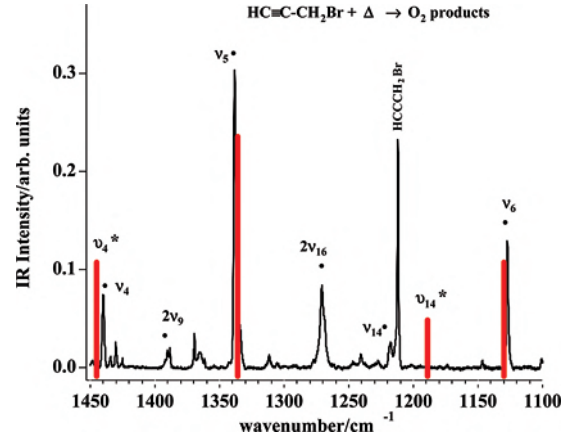

Figure 6. The IR spectrum resulting from addition of O_2 to propargyl radical (generated from $HCCCH_2Br$). The intense red sticks are the predicted bands: υ_4, υ_5, υ_{14}, and υ_6. The calculated anharmonic modes, 4 and 14, are have low intensity (see Table 1) and have been scaled by a factor of 10 to show up in this figure. The scaled bands are marked by an asterisk, υ_4* and υ_{14}*.

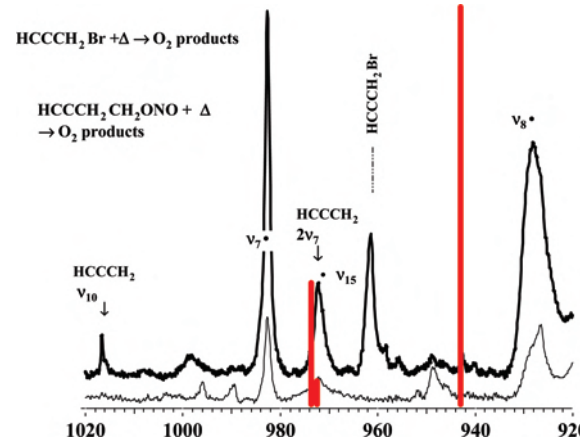

Figure 7. A scan through fingerprint region of the IR spectrum following addition of $HCCCH_2$ to O_2. The top black trace uses $HCCCH_2Br$ as the propargyl precursor and the bottom trace uses $HCCCH_2CH_2ONO$ to generate propargyl radical. The intense red sticks are the predicted CCSD(T)/ANO anharmonic transitions. The calculated modes, υ_7 and υ_{15} are accidentally degenerate at 973 cm^{-1}. For display purposes, we have plotted (υ_7, υ_{15}) split by 1 cm^{-1}.

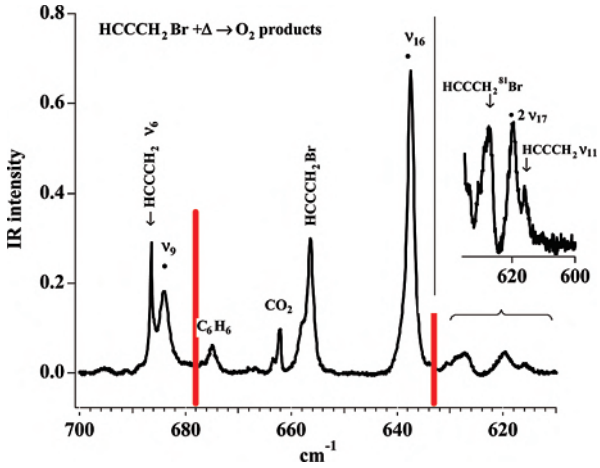

Figure 8. A scan of the low frequency portion of the IR spectrum resulting from addition of O_2 to propargyl radical (generated from $HCCCH_2Br$). The inset at the top of the figure shows the weak overtone of $HCCCH_2OO$, $2\nu_{17}$.

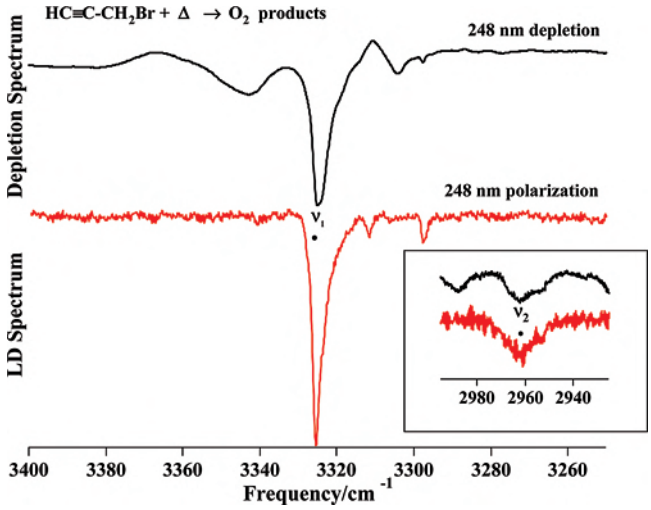

Figure 9. At the top, in black, is an infrared spectrum showing the depletion of matrix isolated propargyl peroxyl radicals in the CH stretching region upon bombardment by 248 nm laser light. On the bottom, in red, is a linear dichroism spectrum of the propargyl radical following matrix depletion by polarized 248 nm light. IR bands of propargyl peroxyl that are a′ polarized will have a negative dichroism while IR features that are a″ polarized will have a positive dichroism. The infrared fundamentals of the propargyl peroxyl radical are marked by bullets (•). An inset figure shows the weakly polarized peak for ν_2.

Discussion

We believe that the propargyl radical is reacting with oxygen in the cryogenic matrix to produce a peroxyl radical, $C_3H_3{-}OO\cdot$. The simplest alkylperoxyl radical, $CH_3{-}OO\cdot$, has four vibrational fundamentals[16,40] that are characteristic peroxyl modes: ν_5(CH_3 rock + OO stretch) = 1180 cm^{-1}, ν_6(CH_3 rock − OO stretch) = 1109 cm^{-1}, ν_7(CO stretch) = 902 cm^{-1}, ν_8(COO bend) = 492 cm^{-1}. Consequently if we are producing a $C_3H_3{-}OO\cdot$ radical, we anticipate the presence of comparable $ROO\cdot$ bands: an O−O stretch between 1100 and 1200 cm^{-1}, a C−O· stretch at approximately 900 cm^{-1}, and a C−O−O· bend at roughly 500 cm^{-1}.

We observe that addition of molecular oxygen to the matrix destroys the propargyl radical. The IR spectra in Figure 2 with characteristic $ROO\cdot$ modes strongly suggests that the $HCCCH_2$ radical has combined with oxygen to produce a peroxyl radical,

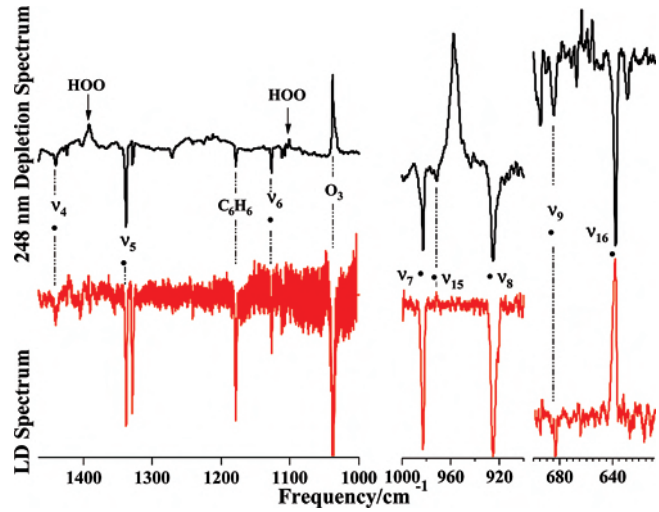

Figure 10. At the top, in black, is an infrared spectrum showing the depletion of matrix isolated propargyl peroxyl radicals, in the fingerprint region upon exposure to 248 nm laser light. On the bottom, in red, is a linear dichroism spectrum of the $HCCCH_2OO$ radical following matrix depletion by polarized 248 nm light. IR bands of propargyl peroxyl that are a′ polarized will have a negative dichroism while IR features that are a″ polarized will have a positive dichroism. The infrared fundamentals of the propargyl peroxyl radical are marked by bullets (•).

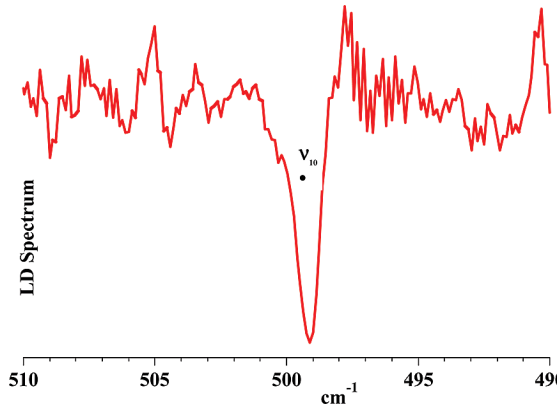

Figure 11. The linear dichroism spectrum of the $HCCCH_2OO$ following matrix depletion by polarized 248 nm light. The $OO{-}CH_2{-}CCH$ bending mode, ν_{10}, is polarized A′.

$C_3H_3OO\cdot$. In Figures 2 and 3, bands at 1127, 928, and 499 cm^{-1} were observed in spectra derived from two different precursors. Guided by the CCSD(T) anharmonic frequencies, these are assigned (Table 1) as ν_6(O−O stretch), ν_8(C-OO stretch), and a mixed bending mode (ν_{10}) that has substantial C−O−O bending character.

We must decide if the peroxyl radical is $H{-}C{\equiv}CCH_2{-}OO\cdot$ or $CH_2{=}C{=}CHOO\cdot$ (or both). One way to differentiate between these two peroxyl radicals is to search for a high frequency CH stretch (>3300 cm^{-1}) which is characteristic of an acetylenic mode (H−C≡C−). The CH portion of the IR spectrum is shown in Figure 4. The bottom portion of this figure shows three different spectra. The two black traces result from addition of the $HCCCH_2$ radical [prepared from $HCCCH_2Br$ (top) or $HCCCH_2CH_2ONO$ (bottom)] to O_2. The red trace corresponds to the $HCCCH_2$ radical as produced from propargyl bromide and shows the two H−C≡C bands for propargyl bromide (ν_1, $H{-}C{\equiv}CCH_2Br$, 3329 cm^{-1}) and the propargyl[5] radical (ν_1, $H - C{\equiv}C{=}CH_2$, 3308 cm^{-1}). In both spectra when $HCCCH_2$ radical is combined with O_2, a new band grows in between

TABLE 2: *trans*-HC≡C−CH_2-OO $\tilde{X}\ ^2A''$ Vibrational Modes

		Ar matrix IR/20 K		calculated ROHF/CCSD(T)/ANO0 anharmonic	
mode	local mode description	ν (cm^{-1})	polarization	adjusted υ (cm^{-1})	adjusted A (km mol^{-1})
a′					
1	C−H st	3326 ± 3	−	3337	44
2	sym CH_2 st	2960 ± 3	−	2951	7
3	C≡C st	2148 ± 1	na	2144	5
4	CH_2 scissors	1440 ± 1	−	1445	2
5	CH_2 wag	1338 ± 1	−	1336	42
6	O−OCH_2CCH st	1127 ± 1	−	1130[a]	20
7	C−C st	982 ± 1	−	973	20
8	O−C st	928 ± 3	−	943	65
9	C≡C−H in-plane bend	684 ± 1	−	678	32
10	O−C−C bend	499 ± 1	−	496	2
11	O−O−C bend	na	na	424	9
12	C−C≡C in-plane deformation	na	na	163[b]	1[b]
a″					
13	asym CH_2 st	na	na	2980	5
14	CH_2 twist	1218 ± 1	na	1189	1
15	CH_2 rock	972 ± 1	+	973[c]	4[c]
16	C≡C−H out-plane bend	637 ± 1	+	633	42
17	C−C≡C out-plane deformation	na	na	309	7
18	O−O−CH_2−C torsion	na	na	73	0

[a] After treatment of $\nu_6 \simeq \nu_9 + \nu_{11}$ resonance. [b] After treatment of $\nu_{12} \simeq 2\nu_{18}$ resonance. [c] After treatment of $\nu_{15} \simeq \nu_9 + \nu_{17}$ resonance.

ν_1(H−C≡CCH_2Br) and ν_1(H−$CCCH_2$). This new band observed at 3326 cm^{-1} only appears when O_2 is added to the matrix and is assigned as the acetylenic H−C stretch, ν_1(H−C≡CCH_2−OO•). The CCSD(T)/ANO prediction for υ_1 is 3337 cm^{-1} and is plotted as the bold red stick in Figure 4. The inset at the top of Figure 4 shows the weak ν_2 symmetric CH_2 absorption at 2960 cm^{-1}; the predicted CCSD(T)/ANO υ_2 is 2951 cm^{-1}. The antisym CH_2 stretching mode, ν_{13}, could not be located. The CCSD(T) calculations in Table 1 predict υ_{13} = 2980 cm^{-1} and A_{13} = 5 km mol^{-1}, slightly less than A_2.

If the carrier of the signal is $HCCCH_2OO$•, we expect a −C≡C− stretch to appear in the IR spectrum. The predicted CCSD(T)/ANO υ_3 is 2144 cm^{-1} and is plotted as a red stick in Figure 5. There are two black traces in this figure showing the spectra resulting from addition of $HCCCH_2$ (produced from $HCCCH_2Br$) to O_2 (top trace) and the spectrum resulting from $HCCCH_2Br$ and propargyl radical by themselves. Intense features for ^{12}CO and ^{13}CO are identified, and a new band at 2148 cm^{-1} grows in to the red of the ν_3(HC≡CCH_2Br) signal. We assign ν_3(HC≡CCH_2OO•) to this new feature.

The clear presence of acetylenic features, ν_1(H−$CCCH_2OO$) and ν_3(HC≡CCH_2OO), identifies the C_3H_3OO adduct as the propargyl peroxyl radical. The HC≡C−CH_2OO• $\tilde{X}\ ^2A''$ radical has 12 a′ ⊕ 6 a″ vibrational modes and we are able to assign most of the major bands. Four fundamental bands, two a′ and two a″, are predicted to lie outside the detection region of the MCT detector used (4000−450 cm^{-1}).

Four fundamentals are shown in Figure 6. A pair of modes, ν_5(CH_2 wag) and ν_6(O−OCH_2CCH st), are intense and thus easy to identify. The other two fundamentals, ν_4(CH_2 scissors) and ν_{14}(CH_2 twist), are weaker. Two features are identified as the overtones $2\nu_9$ and $2\nu_{16}$. The predicted CCSD(T)/ANO levels (υ_4, υ_5, υ_{14}, υ_6) are plotted as red sticks in Figure 6. The calculated intensities for υ_4 and υ_{14} are small and have been scaled by a factor of 10 (marked by an asterisk (*) in the figure) so they will be visible.

The spectra in Figure 7 show intense bands assigned to the HCC−CH_2OO• stretch (ν_7 = 982 cm^{-1}) and the $HCCCH_2$−OO• stretch (ν_8 = 928 cm^{-1}). The CH_2 rocking mode (ν_{15} = 972 cm^{-1}) is very weak and is blended with the $2\nu_7$ overtone of propargyl radical. Figure 2 shows the (ν_7, ν_{15}) pair better. The calculated CCSD(T)/ANO υ_7 and υ_{15} modes are accidentally degenerate at 973 cm^{-1} but are plotted as red sticks split by 1 cm^{-1} in Figure 7. The $OOCH_2CC$≡C−H bending modes, ν_9 = 684 and ν_{16} = 637 cm^{-1}, are shown in Figure 8. At the top right is an inset which shows a feature at 620 cm^{-1}; this is assigned as the overtone of C−C≡C out-plane deformation, $2\nu_{17}$ = 620 cm^{-1}.

Figures 9−11 depict the depletion and linear dichroism spectra for the H−C≡CCH_2−OO• radical. In the CH stretching region ν_1 and ν_2 demonstrate negative dichroism at 3326 ± 6 and 2961 ± 8 cm^{-1} characteristic of a′ modes (Figure 9). Seven additional propargyl peroxyl bands demonstrated negative LD (Figure 10) and are assigned as a′ modes: ν_4, ν_5, ν_6, ν_7, ν_8, ν_9, and ν_{10}. Vibrations ν_{15} and ν_{16} have positive LD, and are thus a″ modes. The weak $OOCH_2CC$≡CH mode (ν_3) and the CH_2-twisting mode (ν_{14}) were not detected in an LD experiment. To collect such spectra, IR signals are first depleted by as much as 75%. The wire grid polarizers tend to attenuate signals even further, thus making weaker signals difficult to observe over the noise.

The H−C≡C≡CH_2 radicals are reactive radicals and can dimerize. IR signals from benzene were clearly observed in some of the matrix spectra (for example, Figure 8). In previous work[5] we observed propargyl radical chemistry by observing (CH_2=C=CH_2, HC≡C−CH_3 and benzene) in both matrix IR spectra and in gas phase photoionization mass spectra. Their presence in both experiments indicates that radical/radical dimerization and H-abstraction reactions are occurring in the hyperthermal nozzle.

The final set of matrix assignments for *trans*-H−C≡CCH_2−OO• are collected in Table 2. We have adopted the half-full-width at half-maximum ($^1/_2$ fwhm) intensity as a measure of the uncertainty for the matrix frequency. These uncertainties are somewhat subjective because we have little understanding of the complex line shapes that are observed. An additional difficulty is that several of the $HCCCH_2OO$ modes are blended with other peaks in the spectrum.

TABLE 3: Comparison of CH_3OO $\tilde{X}\,^2A''$ Matrix vs Gas-Phase Vibrational Modes

		matrix[16] (cm^{-1})	gas phase[40] (cm^{-1})
a′			
ν_1	CH_3 symmetric stretch	3032	3033 ± 1
ν_2	CH_3 total symmetric stretch	2954	2954 ± 1
ν_3	CH_3 deformation	1448	1453 ± 2
ν_4	CH_3 umbrella	1410	1408 ± 1
ν_5	CH_3 rock+OO stretch	1180	1183 ± 1
ν_6	CH_3 rock+OO stretch	1109	1117 ± 2
ν_7	CO stretch	902	na
ν_8	COO bend	492	na
a″			
ν_9	CH_3 asymmetric stretch	3024	3020 ± 2
ν_{10}	CH_3 asym. deformation	1434	1441 ± 1
ν_{11}	CH_2 wag	na	na
ν_{12}	CH_3 torsion	na	na

It would be helpful to estimate a complete set of internally consistent, reliable vibrational frequencies for the gas-phase $HCCCH_2OO$ radical. There are no gas-phase observations of the propargyl peroxyl radical. Jacox has reviewed the matrix shifts for a large number of diatomic and small polyatomic free radicals and ions trapped in Ne and Ar matrices.[41,42] She concluded that for polyatomic free radicals in Ar matrices the frequency shift is generally less than 1% and usually to the red.

In an earlier study of the allyl radical,[43] we observed the five CH stretching modes of CH_2CHCH_2. High resolution laser spectroscopy[44–46] subsequently also detected all five as well. For allyl radical, CH_2CHCH_2, the shifts (gas-matrix) are $\Delta\nu_1$ (25 cm^{-1}), $\Delta\nu_2$ (18 cm^{-1}), $\Delta\nu_3$ (4 cm^{-1}), $\Delta\nu_{13}$ (4 cm^{-1}), and $\Delta\nu_{14}$ (0 cm^{-1}). A similar result was found for the phenyl radical, C_6H_5. Almost a decade ago a hyperthermal nozzle was used[47] to deposit phenyl radical in a matrix, and 24 of 27 total vibrational modes were observed. Recent tunable-difference-frequency laser studies[48] of jet-cooled C_6H_5 radicals have reported $\nu_{19}(C_6H_5) = 3071.8904 \pm 0.0010$ cm^{-1}. Consequently for phenyl radical, the gas-to-matrix shift is $\Delta\nu_{19}$ (0.9 cm^{-1}).

An earlier IR study of the methyl peroxyl radical[16] produced the CH_3OO radical by condensation of CH_3 with O_2 in a cryogenic matrix. Recently it has become possible to assess the gas-matrix shifts of the CH_3OO radical. A step-scan Fourier-transform spectrometer coupled with a multipass absorption cell was employed[40] to record time-resolved IR absorption spectra of reaction intermediates resulting from addition of CH_3 to O_2. That paper observed rotationally resolved bands for several modes of the CH_3OO* radical. A comparison of the matrix values versus the gas-phase assignments is shown in Table 3. Most of the matrix values are within a few cm^{-1} of the gas-phase modes; the biggest discrepancy is 8 cm^{-1} for ν_6. Consequently we believe that all of the matrix frequencies for the propargyl radical are within ≤1% of the true, gas phase frequencies.

What are the likely pathways for $HCCCH_2$ to react with O_2? The thermochemistry of reactions 2−6 has been considered earlier but should be slightly revised. Table 4 lists the experimental enthalpies for reaction of $HCCCH_2$ with O_2. For most channels, the ΔE_{calcd} values[2] are close to the range spanned by the $\Delta_{rxn}H_{298}$ uncertainties. It is also encouraging that the CBS/QB3 "semi-empirical" calculations correctly predict $\Delta H_{298}(HCCCH_2{-}OO)$ to be 19 ± 1 kcal mol^{-1} in good agreement with the flow tube results. The QCISD(T,full)/6-311++G(3df,2pd) calculations correctly predict that the activation barriers for O_2 addition to $HCCCH_2$ favor the propargyl peroxyl radical, $E_a(8) < E_a(7)$. The QCISD(T,full) estimate for

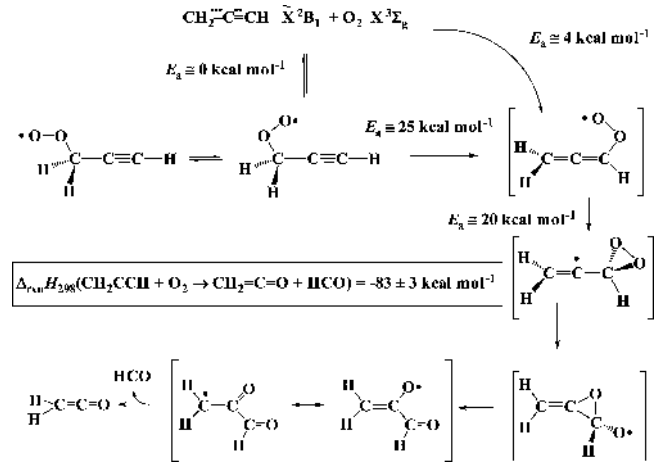

Figure 12. A possible mechanism for the reaction,

$$HC{\equiv}C{-}CH_2 + O_2 \rightarrow CH_2{=}C{=}O + HCO$$

This composite figure is based on previous electronic structure calculations.[2,49,50] The thermochemistry is from Table 4.

TABLE 4: Experimental Thermochemistry of the $HCCCH_2$ + O_2 Reaction

reaction	$\Delta_{rxn}H_{298}$ (kcal mol^{-1})	reference
$HCCCH_2 + O_2 \rightarrow HC{\equiv}CCH_2OO$	−19 ± 1	13
$HCCCH_2 + O_2 \rightarrow CH_2{=}C{=}O + HCO$	−83 ± 3	51–54
$HCCCH_2 + O_2 \rightarrow CH_3CO + CO$	−111 ± 3	53, 55
$HCCCH_2 + O_2 \rightarrow CH_2CHO + CO$	−106 ± 4	53, 56–58
$HCCCH_2 + O_2 \rightarrow HCHO + HCCO$	−67 ± 4	53, 59
$HCCCH_2 + O_2 \rightarrow CH_2CH + CO_2$	−105 ± 3	54, 60
$HCO \rightarrow H + CO$	15.6 ± 0.1	52

$E_a(8)$ is 3.7 kcal mol^{-1} but Hahn et al. empirically[2] reduced $E_a(8)$ to −0.2 kcal mol^{-1}. Our experimental findings agree with this revision. The $HC{\equiv}CCH_2OO$ radicals in Figures 2−11 are produced by addition of $HCCCH_2$ radicals with O_2 in an Ar matrix at 20 K. Exothermic bimolecular reactions at such low temperatures cannot have non-negligible activation barriers. Even though the CBS/QB3 calculations predict $\Delta H_{298}(CH_2{=}C{=}CH{-}OO)$ to be 21 ± 1 kcal mol^{-1}, we find no experimental evidence for the formation of the allenyl peroxyl radical. This is consistent with the prediction of Hahn et al.[2] that $E_a(7) > 0$.

On the basis of the theoretical results, earlier experimental findings, and this work, we can produce a plausible reaction mechanism for the reaction of $HCCCH_2$ and O_2; this is shown in Figure 12. At low temperatures, propargyl radical reversibly adds to oxygen to produce the $HC{\equiv}CCH_2OO$ radical. At higher temperatures above 350 K, propargyl radicals combine with oxygen to produce chemically activated allenyl peroxyl radicals, $(CH_2{=}C{=}CH{-}OO)$*. On the basis of the calculations of Hahn et al.[2] and Carpenter's insights to dioxiranyl radicals,[49,50] a mechanism for reaction 2 producing $CH_2{=}C{=}O$ + HCO is sketched in Figure 12. Ketene and the formyl radical were the only products detected by Slagle and Gutman[13] but their PIMS spectrometer could not detect CO or CO_2. Dong et al. clearly observed IR emission signals[14] for HCO*, CO_2*, and CO* from the reaction of $HCCCH_2$ with O_2 at low pressures (0.3 Torr). The addition of 2 Torr Ar buffer gas completely quenched signals from CO_2*. All of these products can be rationalized by Figure 12. Table 4 shows $\Delta_{rxn}H_{298}(HCCCH_2 + O_2 \rightarrow CH_2CO + HCO) = -83 \pm 3$ kcal mol^{-1}. Consequently it is likely that the products $CH_2{=}C{=}O$* and HCO* are chemically activated. Because $\Delta H_{298}(H{-}CO)$ is only 15.6 ± 0.1 kcal mol^{-1}, it seems

likely that much of the CO* could be derived from HCO*. The intermediate dioxiranyl radical is a possible source for the CO_2* detected by Dong et al.

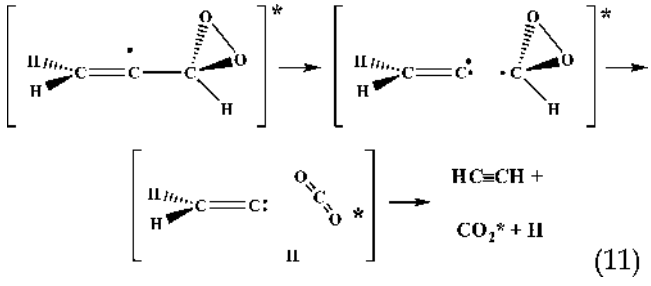

(11)

Equation 11 is consistent with the observation[14] that increasing the buffer gas pressure suppresses emission from CO_2*. The dioxiranyl radical in eq 11 was computed to be an important intermediate by Dong et al. (designated **IM2** in Figure 4 of ref 14). The pathways in Figure 4 in ref 14 are the result of UB3LYP/6-31+G(d,p) electronic structure calculations. These calculations argue that the $^2A'$ dioxiranyl radical rearranges to the vinyl oxycarbonyl radical (designated **IM7** in Figure 4 of ref 14) that decarboxylates to the vinyl radical. The CH_2=CH radical could decompose to acetylene and a H atom.

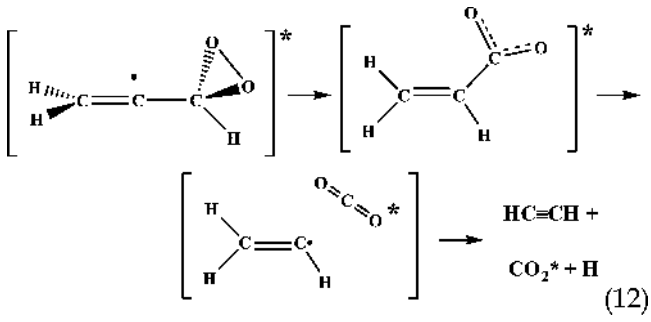

(12)

The differences between the pathways in eq 11 and 12 are based on the observation that alkyloxycarbonyl radicals, RCO_2, are not bound species. They spontaneously fragment carbon dioxide: $RCO_2 \rightarrow R + CO_2$. The HCO_2, CH_3CO_2, and $C_6H_5CO_2$ radicals have been studied by photodetachment: $RCO_2^- + \hbar\omega_{266\ nm} \rightarrow RCO_2 + e^-$. The only oxycarbonyl radical that has been isolated is the oxybenzoyl radical, $C_6H_5CO_2$, which was observed by EPR in a low temperature crystal. It is unlikely that the UB3LYP/6-31+G(d,p) calculations will properly characterize RCO_2 radicals and we think that eq 11 is a more likely path for the production of CO_2* observed by Dong. et al.[14]

Conclusions

Propargyl radicals have been produced through the use of a supersonic hyperthermal nozzle. These radicals were able to combine with O_2 in a cold Ar matrix, indicating that the reaction between propargyl radical and O_2 occurs without a barrier. Vibrational bands characteristic of all R-OO species were positively identified for the new species, confirming its identity as a peroxyl radical. The high frequency acetylenic stretch detected in the experiment shows that the addition product is the propargyl peroxy (HC≡CCH_2−OO) conformer. No peaks corresponding to the allenyl peroxyl radical (CH_2=C=CH−OO) have been detected. Although previous calculations[2] have found allenyl peroxyl to be >5 kcal mol^{-1} more stable than propargyl peroxyl, we find no prominent spectroscopic evidence for the CH_2CCHOO peroxyl radical.

Acknowledgment. This work was supported by grants from the United States Department of Energy (DE-FG02-93ER14364) and the National Science Foundation (CHE-9813659) (G.B.E., J.F.S.), the Department of Energy, Basis Energy Sciences (DE-FG02-07ER15884), and the Robert A. Welch Foundation (J.F.S.). X.Z. would like to acknowledge support from a NASA postdoctoral fellowship.

References and Notes

(1) Westmoreland, P. R.; Dean, A. M.; Howard, J. B.; Longwell, J. P. *J. Phys. Chem.* **1989**, *93*, 8171.
(2) Hahn, D. K.; Klippenstein, S. J.; Miller, J. A. *Faraday Discuss.* **2001**, *119*, 79.
(3) Roberts, J. D.; Caserio, M. *Organic Chemistry*; W. A. Benjamin: Menlo Park, CA, 1977.
(4) Kasai, P. H. *J. Am. Chem. Soc.* **1972**, *94*, 5950.
(5) Jochnowitz, E. B.; Zhang, X.; Nimlos, M. R.; Varner, M. E.; Stanton, J. F.; Ellison, G. B. *J. Phys. Chem. A* **2005**, *109*, 3812.
(6) Goddard III, W. A.; Harding, L. B. *Annu. Rev. Phys. Chem.* **1978**, *29*, 363.
(7) Blanksby, S. J.; Ellison, G. B. *Acc. Chem. Res.* **2003**, *36*, 255.
(8) Howe, P. T.; Fahr, A. *J. Phys. Chem. A* **2003**, *107*, 9603.
(9) Morter, C. L.; Farhat, S. K.; Adamson, J. D.; Glass, G. P.; Curl, R. F. *J. Phys. Chem.* **1994**, *98*, 7029.
(10) Atkinson, D. B.; Hudgens, J. W. *J. Phys. Chem. A* **1999**, *103*, 4242.
(11) DeSain, J. D.; Taatjes, C. A. *J. Phys. Chem. A* **2003**, *107*, 4843.
(12) Shafir, E. V.; Slagle, I. R.; Knyazev, V. A. *J. Phys. Chem. A* **2003**, *107*, 8893.
(13) Slagle, I. R.; Gutman, D. *Proc. Combust. Inst.* **1986**, *21*, 875.
(14) Dong, F.; Wang, S. F.; Kong, F. A. *J. Phys. Chem. A* **2003**, *107*, 9374.
(15) Minsek, D. W.; Chen, P. *J. Phys. Chem.* **1990**, *94*, 8399.
(16) Nandi, S.; Blanksby, S. J.; Zhang, X.; Nimlos, M. R.; Dayton, D. C.; Ellison, G. B. *J. Phys. Chem. A* **2002**, *106*, 7547.
(17) Pedley, J. B.; Naylor, R. D.; Kirby, S. P. *Thermochemistry of Organic Compounds*, 2nd ed.; Chapman and Hall: New York, 1986. The simplest nitrite (CH_3O-NO) has well known thermochemistry. The $\Delta_f H_{298}(CH_3ONO)$ is -15.9 ± 0.2 kcal mol^{-1} while Ervin and DeTuri report $\Delta_f H_{298}(CH_3O)$ as 4.3 ± 0.7 kcal mol^{-1}. Consequently $\Delta H_{298}(CH_3O-NO) = 42.0 \pm 0.7$ kcal mol^{-1}.
(18) Zhang, X.; Friderichsen, A. V.; Nandi, S.; Ellison, G. B.; David, D. E.; McKinnon, J. T.; Lindeman, T. G.; Dayton, D. C.; Nimlos, M. R. *Rev. Sci. Instrum.* **2003**, *74*, 3077.
(19) Becke, A. D. *J. Chem. Phys.* **1993**, *98*, 5648.
(20) Lee, C. T.; Yang, W. T.; Parr, R. G. *Phys. Rev. B* **1988**, *37*, 785.
(21) Petersson, G. A. *Complete Basis Set Methods*; ACS Symposium Series, Vol. 677; W. A. Benjamin: Washington, DC, 1998.
(22) Montgomery, J. A.; Frisch, M. J.; Ochterski, J. W.; Petersson, G. A. *J. Chem. Phys.* **1999**, *110*, 2822.
(23) Lee, T. J.; Scuseria, G. E. In *Quantum Mechanical Electronic Structure Calculations with Chemical Accuracy*; Langhoff, S. R., Ed.; Kluwer: Dordrecht, The Netherlands, 1995.
(24) Bartlett, R. J. In *Modern Electronic Structure Theory, Part II*; Yarkony, D. R., Ed.; World Scientific: Singapore, 1995.
(25) Gauss, J. Coupled Cluster Theory. In *Encyclopedia of Computational Chemistry*; Schleyer, P., Ed.; Wiley: New York City, 1998.
(26) Crawford, T. D.; Schaefer, H. F., III. *Rev. Comp. Chem.* **1999**, *14*, 36.
(27) Stanton, J. F.; Gauss, J.; Harding, M. E.; Szalay, P. G. *CFOUR, Coupled Cluster Techniques for Computational Chemistry*; 2009; . http://www.cfour.de.
(28) Raghavachari, K.; Trucks, G. W.; Pople, J. A.; Head-Gordon, M. *Chem. Phys. Lett.* **1989**, *157*, 479.
(29) Raghavachari, K.; Trucks, G. W.; Pople, J. A.; Replogle, E. *Chem. Phys. Lett.* **1989**, *158*, 207.
(30) Almlof, J.; Taylor, P. R. *J. Chem. Phys.* **1987**, *86*, 4070.
(31) Gauss, J.; Stanton, J. F. *Chem. Phys. Lett.* **1997**, *276*, 70.
(32) Stanton, J. F.; Lopreore, C. L.; Gauss, J. *J. Chem. Phys.* **1998**, *108*, 7190.
(33) Blanksby, S. J.; Ramond, T. M.; Davico, G. E.; Nimlos, M. R.; Kato, S.; Bierbaum, V. M.; Lineberger, W. C.; Ellison, G. B.; Okumura, M. *J. Am. Chem. Soc.* **2001**, *123*, 9585.
(34) Ramond, T. M.; Blanksby, S. J.; Kato, S.; Bierbaum, V. M.; Davico, G. E.; Schwartz, R. L.; Lineberger, W. C.; Ellison, G. B. *J. Phys. Chem. A* **2002**, *106*, 9641.

(35) Pushkarsky, M. B.; Zalyubovsky, S. J.; Miller, T. A. *J. Chem. Phys.* **2000**, *112*, 10695.
(36) Glover, B. G.; Miller, T. A. *J. Phys. Chem. A* **2005**, *109*, 11191.
(37) Tarczay, G.; Zalyubovsky, S. J.; Miller, T. A. *Chem. Phys. Lett.* **2005**, *406*, 81.
(38) Just, G. M. P.; Sharp, E. N.; Zalyubovsky, S. J.; Miller, T. A. *Chem. Phys. Lett.* **2006**, *417*, 378.
(39) Rupper, P.; Sharp, E. N.; Tarczay, G.; Miller, T. A. *J. Phys. Chem. A* **2007**, *111*, 832.
(40) Huang, D. R.; Chu, L. K.; Lee, Y. P. *J. Chem. Phys.* **2007**, *127*, 234318.
(41) Jacox, M. E. *J. Mol. Spectrosc.* **1985**, *113*, 286.
(42) Jacox, M. E. *Chem. Phys.* **1994**, *189*, 149.
(43) Nandi, S.; Arnold, P. A.; Carpenter, B. K.; Nimlos, M. R.; Dayton, D. C.; Ellison, G. B. *J. Phys. Chem. A* **2001**, *105*, 7514.
(44) Uy, D.; Davis, S.; Nesbitt, D. J. *J. Chem. Phys.* **1998**, *109*, 7793.
(45) DeSain, J. D.; Thompson, R. I.; Sharma, S. D.; Curl, R. F. *J. Chem. Phys.* **1998**, *109*, 7803.
(46) Han, J. X.; Utkin, Y. G.; Chen, H. B.; Burns, L. A.; Curl, R. F. *J. Chem. Phys.* **2002**, *117*, 6538.
(47) Friderichsen, A. V.; Radziszewski, J. G.; Nimlos, M. R.; Winter, P. R.; Dayton, D. C.; David, D. E.; Ellison, G. B. *J. Am. Chem. Soc.* **2001**, *123*, 1977.
(48) Sharp, E. N.; Roberts, M. A.; Nesbitt, D. J. *Phys. Chem. Chem. Phys.* **2008**, *10*, 6592.
(49) Carpenter, B. K. *J. Am. Chem. Soc.* **1993**, *115*, 9806.
(50) Carpenter, B. K. *J. Phys. Chem. A* **2001**, *105*, 4585.
(51) Chuang, M. C.; Foltz, M. F.; Moore, C. B. *J. Chem. Phys.* **1987**, *87*, 3855.
(52) Terentis, A. C.; Kable, S. H. *Chem. Phys. Lett.* **1996**, *258*, 626. This paper is an improvement on the photodissociation results of Chuang et al. State-to-state dynamics of the gas phase reaction $H_2CO + h\nu \rightarrow H + HCO$ find $\Delta\nu_0(H-CHO) = 30328.5 \pm 0.5\ cm^{-1}$. Correcting to 298 K one finds $\Delta H_{298}(H-CHO) = 88.144 \pm 0.008$ kcal mol^{-1}. Use of the heat of formation from Pedley et al., $\Delta_f H_{298}(CH_2O) = -26.0 \pm 0.1$ kcal mol^{-1}, yields $\Delta_f H_{298}(HCO) = 10.1 \pm 0.1$ kcal mol^{-1}.
(53) Robinson, M. S.; Polak, M. L.; Bierbaum, V. M.; DePuy, C. H.; Lineberger, W. C. *J. Am. Chem. Soc.* **1995**, *117*, 6766. $\Delta H_{298}(H-CH_2CCH) = 90 \pm 3$ kcal mol^{-1}; $\Delta_f H_{298}(CH_2CCH) = 82.5 \pm 3.0$ kcal mol^{-1}.
(54) Ervin, K. M.; DeTuri, V. F. *J. Phys. Chem. A* **2002**, *106*, 9947.
(55) Niiranen, J. T.; Gutman, D.; Krasnoperov, L. N. *J. Phys. Chem.* **1992**, *96*, 5881. $\Delta H_{298}(CH_3CO\text{-}H) = 89.3 \pm 0.4$ kcal mol^{-1}; use of value from Pedley et al for $\Delta_f H_{298}(CH_3CHO) = -39.7 \pm 0.1$ kcal mol^{-1} leads to $\Delta_f H_{298}(CH_3CO) = -2.4 \pm 0.3$ kcal mol^{-1}.
(56) Bartmess, J. E.; Scott, J. A.; McIver, R. T. *J. Am. Chem. Soc.* **1979**, *101*, 6046. Application of the acidity/E_A cycle (described by Berkowitz et al.) combine the $E_A(CH_2CHO)$ from Mead et al. and $\Delta_{acid}H_{298}(H-CH_2CHO)$ to find the $\Delta_f H_{298}(CH_2CHO) = 3 \pm 2$ kcal mol^{-1}.
(57) Mead, R. D.; Lykke, K. R.; Lineberger, W. C.; Marks, J.; Brauman, J. I. *J. Chem. Phys.* **1984**, *81*, 4883.
(58) Berkowitz, J.; Ellison, G. B.; Gutman, D. *J. Phys. Chem.* **1994**, *98*, 2744.
(59) Oakes, J. M.; Jones, M. E.; Bierbaum, V. M.; Ellison, G. B. *J. Phys. Chem.* **1983**, *87*, 4810. The acidity/E_A cycle was used to find $\Delta H_{298}(H-CHCO) = 105.9 \pm 2.1$ kcal mol^{-1}. Use of the $\Delta_f H_{298}(CH_2{=}C{=}O) = -11.4 \pm 0.4$ from Pedley et al. leads to $\Delta_f H_{298}(HCCO) = 42.4 \pm 2.1$ kcal mol^{-1}.
(60) Ervin, K. M.; Gronert, S.; Barlow, S. E.; Gilles, M. K.; Harrison, A. G.; Bierbaum, V. M.; Charles, H. DePuy; Lineberger, W. C.; Ellison, G. B. *J. Am. Chem. Soc.* **1990**, *112*, 5750. The acidity/E_A cycle is used to find $\Delta H_{298}(CH_2CH-H) = 110.7 \pm 0.6$ kcal mol^{-1}. Use of the value from Pedley et al. for $\Delta_f H_{298}(CH_2CH_2) = 12.5 \pm 0.1$ kcal mol^{-1} leads to $\Delta_f H_{298}(CH_2CH) = 71.1 \pm 0.7$ kcal mol^{-1}.

JP907806G